



Revealing the influence of the compression mechanism on the electronic structure and the related properties of CrF₃



A.H. Reshak ^{a, b, *}

^a New Technologies – Research Centre, University of West Bohemia, Univerzitni 8, 306 14 Pilsen, Czech Republic

^b Center of Excellence Geopolymer and Green Technology, School of Material Engineering, University Malaysia Perlis, 01007 Kangar, Perlis, Malaysia

ARTICLE INFO

Article history:

Received 17 August 2015
Received in revised form
8 October 2015
Accepted 5 November 2015
Available online 11 November 2015

Keywords:

Ambient pressure
High pressure
Strain
CrF₃
DFT
Optical properties

ABSTRACT

The influence of the compression mechanism on the unit cell of CrF₃ is investigated by means of density functional theory. The experimental lattice parameters under different pressure values starting from the ambient pressure up to 9.12 GPa were optimized so as to relax the crystalline structures. To ascertain the effect of pressure on the structural properties, the electronic band structure, density of states, Fermi surface and chemical bonding were calculated. The electronic band structure explored the metallic nature of CrF₃ and the density of states confirmed that. The density of states at Fermi level and the specific heat coefficient were obtained at different pressure values which show significant reduction occurs with increasing the pressure. It has been found that the pressure cause to push Cr-s/p orbitals to hybridize with F-s orbital at high energy region between 14.0 eV and 15.0 eV. Also it cause a small octahedral strain and reduce the bond lengths and angles in good agreement with the experimental values. Increasing the pressure leads to change the shape of Fermi surface. Further deep insight into the electronic structure can be obtained from the optical dielectric functions. The calculated optical properties confirmed that the pressure cause significant influence of the structure of CrF₃.

© 2015 Elsevier B.V. All rights reserved.

1. Introduction

Chromium(III) fluoride is an inorganic compound with the chemical formula CrF₃ as well as several related hydrates. The compound CrF₃ is a green crystalline solid that is insoluble in common solvents, but the colored hydrates [Cr(H₂O)₆]F₃ and [Cr(H₂O)₆]F₃·3H₂O are soluble in water. It has been found that the trihydrate is green and the hexahydrate is violet. The anhydrous form sublimates at 1100–1200 °C. The volumetric mass density of the anhydrous form is about 3.8 g/cm³ while for the trihydrate form is 2.2 g/cm³ [1]. The chromium(III) compounds feature octahedral Cr centers. It has been noticed that in the anhydrous form, the six coordination sites are occupied by fluoride ligands that bridge to adjacent Cr centers. Whereas in the hydrates, some or all of the fluoride ligands are replaced by water [1]. The chromium(III) fluoride is produced from the reaction of chromium(III) oxide and hydrofluoric acid [2], while the anhydrous form is produced from hydrogen fluoride and chromic chloride [3]. Chromium(III) fluoride

is not heavily used, but finds some applications as a mordant in textiles and as a corrosion inhibitor [1–3].

The metal trifluorides CrF₃ having the formula MX₃ with rhombohedral structure was experimentally investigated by X-ray diffraction [4,5]. It has been reported that CrF₃ is composed of corner-sharing CrF₆ octahedra which is structurally related to the perovskite type materials and each CrF₆ octahedron consist of two F–F distances [4,5]. Jorgensen et al. [6] have used the time-of-flight neutron powder diffraction to investigate the structure of CrF₃ under pressure's values vary between ambient pressure and 9.12 GPa. A small octahedral strain was found with increasing the pressure. They reported that within the investigated pressure range there is volume reduction during the rotation of the CrF₆ octahedra with decreasing the bond angles of Cr–F–Cr [6]. Several research work have been done on materials having the same structure [4–15]. Recently Reshak [16] has investigated the influence of the compression mechanism on the transport properties of CrF₃. To the best of our knowledge, there are no previous experimental or theoretical results for the electronic band structure, density of states, Fermi surface and the electronic charge density distribution of CrF₃ have appeared in the literature. Therefore, as a natural extension to existence information on CrF₃ [1–14,16] a detailed

* New Technologies – Research Centre, University of West Bohemia, Univerzitni 8, 306 14 Pilsen, Czech Republic.

E-mail address: maalidph@yahoo.com.

depiction of the electronic structural and the optical properties of CrF_3 using full potential method is timely and would bring us important insights in understanding the influence of the compression mechanism on the unit cell of CrF_3 and hence the resulting properties. First-principles calculation is one strong and useful tool to predict the crystal structure and its properties related to the electron configuration of a material before its synthesis [17–20].

2. Details of calculation

The influence of the comparison mechanism on the electronic structure, electronic charge density distribution and optical properties of CrF_3 were comprehensively investigated by means of density functional theory (DFT). It has been reported that the CrF_3 crystallizes in hexagonal structural with space group $R\bar{3}c$. Fig. 1 illustrated the crystal structure of CrF_3 . It is clear that the compound feature octahedral Cr centers, the six coordination sites are occupied by fluoride ligands that bridge to adjacent Cr centers [1,6]. The experimental lattice parameters at pressure vary between ambient pressure and 9.12 GPa [6] were utilized to optimize the lattice constant using Perdew, Burke and Ernzerhof generalized gradient approximation (*PBE-GGA*) [21]. Using the optimized lattice constants at different pressures, the experimental atomic positions [6] were optimized by minimizing the forces acting on each atom by using *PBE-GGA* [16]. Fig. 2(a) reveal that the optimized lattice constants (**a** and **c**) agree well with the experimental one [6]. It has been noticed that increasing the pressure cause to decrease the lattice parameter **a**-by around 7.2% and increase **c**-by around 0.17% [16]. The **c**-parameter increases by around 0.17% up to 3.43 GPa. This associated with the small distortion in the CrF_6 octahedra. Shedding more pressure leads to decrease the **c**-parameter [16]. The experimental [6] and our theoretical reduced volume (V/V_0) as function of pressure (GPa) is shown in Fig. 2(b), it has been found that volume reduction occurs through the rotation of CrF_6 around **c**-axis, that is attributed to the differences in the pressure dependence of **a**- and **c**-lattice constants where **c**-lattice constant show less pressure dependence than **a**-lattice constant as it is clear from Fig. 2(a). In addition, we have plotted the calculated volume (\AA^3) vs. energy (Ry) in Fig. 2(c). These figures exhibit that no phase transition occurs within the investigated pressure range in good agreement with the experimental finding of Jorgensen et al. [6]. As it has been stated by Jorgensen et al. the volume reduction is achieved through rotation of the CrF_6 octahedra around the **c**-axis

direction [6].

The full potential linear augmented plane wave plus local orbitals (*FPLAPW+lo*) method in a scalar relativistic version as embodied in the *WIEN2k* code [22] was employed. The exchange-correlation (*XC*) potential was solved by using *PBE-GGA* which is based on *XC* energy optimization to calculate the total energy. The Kohn–Sham equations are solved using a basis of linear *APW*s. The potential and charge density in the muffin-tin (*MT*) spheres are expanded in spherical harmonics with $l_{max} = 8$ and non-spherical components up to $l_{max} = 6$. The *MT* radii for Cr and F atoms are 1.83 a.u. and 1.74 a.u. for the pressures 0.0001, 1.01 and 1.84 GPa, 1.82 a.u., 1.73 a.u. for the pressures 3.43, 5.43 and 7.46 GPa, finally 1.81 a.u. and 1.72 a.u. for the pressures 8.56 and 9.12 GPa [16]. Self-consistency is obtained using 300 *k* points in the irreducible Brillouin zone (*IBZ*). The self-consistent calculations are converged since the total energy of the system is stable within 0.00001 Ry. The electronic band structures and the related properties were performed within 800 *k* points in *IBZ*.

3. Results and discussion

3.1. Electronic band structure and density of states

To ascertain the effect of pressure on the electronic band structure of CrF_3 , the electronic band structures were calculated at the same pressure values which were experimentally investigated as shown in Fig. 3 and the Supplementary Materials Fig. S1(a–c). It is clear that the pressure cause significant influence on the bands locations below and above the Fermi level (E_F) resulting in some modification in the ground state properties [16]. Further investigation to ascertain the effect of pressure on the electronic structure and related properties, the total density of states (*TDOS*) was calculated as illustrated in Fig. 4(a) which exhibit that the pressure push the bands below and above E_F away from E_F below -4.0 eV and above -1.0 eV. That is attributed to the fact that in the solid state system the bonding states and anti-bonding states are closely related to the strength of the orbital splitting. Applying external pressure will lead to compress the chemical bonding, resulting in an increasing in the orbital splitting. Therefore, the bonding states will go deeper into the lower energy level and enhance the energy level of the anti-bonding states [16].

Further, we have investigated the pressure's influence on the positions of Cr-s/p/d and F-s/p orbitals. As prototype we have presented the projected density of states (*PDOS*) at ambient

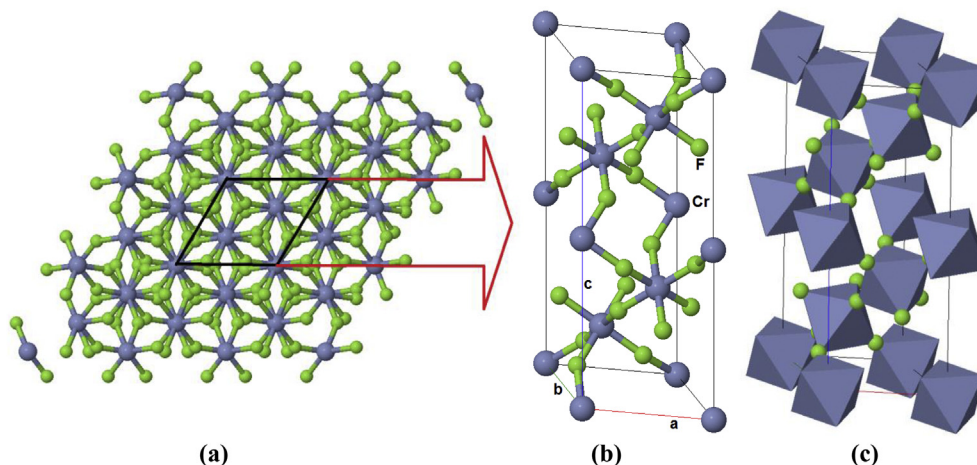


Fig. 1. (a) illustrated the crystal structure of CrF_3 ; (b–c) unit cell of CrF_3 , it is clear the compound feature octahedral Cr centers, the six coordination sites are occupied by fluoride ligands that bridge to adjacent Cr centers.

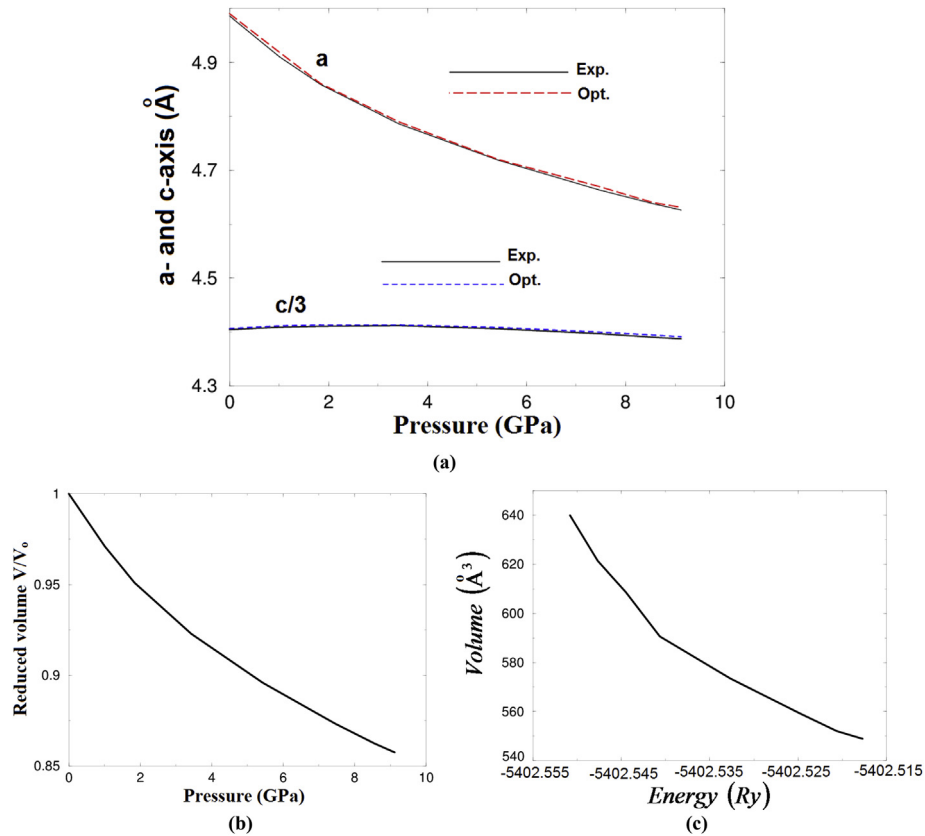


Fig. 2. (a) The experimental [6] and optimized lattice parameters a (Å) and c (Å) as function of pressure (GPa), c is divided by three in order to be in concordance with experimental curve. It has been noticed that increasing the pressure cause to decrease the lattice parameter a -by around 7.2% and increase c -by around 0.17%. The c -parameter increases by around 0.17% up to 3.43 GPa. This associated with the small distortion in the CrF_6 octahedra. Shedding more pressure lead to decrease the c -parameter; (b) The experimental and the calculated reduced volumes (V/V_0) as function of pressure (GPa); (c) The calculated volume (Å^3) as function of energy (Ry).

pressure (we call it as case 1) and at high pressure (case 8) as shown in Fig 4(b)–(e). After carefully looking at Fig. 4(b) and (c) we can see there is significant influence on the peaks positions, peaks heights, the states/bands dispersion and the hybridizations of the Cr-s/p and F-s orbitals. It is clear that the high pressure leads to compress the structures which are extended between 4.5 eV and 17.5 eV (Fig. 4(b)) to be situated in the region between 5.0 eV and 15.75 eV (Fig. 4(c)), with significant reduction in the peaks heights. Also it cause to push Cr-s/p orbitals to hybridized with F-s orbital at high energy region between 14.0 eV and 15.0 eV. The pressure push the structure around 2.0 eV (Fig. 4(b)) to be situated at 2.25 eV with increasing the peak height of F-s orbital (Fig. 4(c)). Whereas below E_F the pressures cause to shifts the structure extended from -8.5 eV up to -4.0 eV (Fig. 4(b)) to be located between -9.0 eV and -5.0 eV with reducing the peak heights of Cr-s/p orbitals (Fig. 4(c)). Fig. 4(d) and (e) clearly show that the pressure have significant influence on the Cr-d and F-p orbitals, it leads to reduce the bandwidth and the peak height of Cr-d orbital around E_F . Also the pressure cause to push the structures of Cr-d and F-p which are extended between -8.5 eV and -4.5 eV (Fig. 4(d)) to be located between -9.0 eV and -5.0 eV (Fig. 4(e)). We have calculated $N(E_F)$, the DOS at E_F , for CrF_3 at the investigated pressure range. Then from the existence information about $N(E_F)$ we can obtain the electronic specific heat coefficient (γ), as described in detail previously [23]. These values are presented in Table 1, it is clear that the compression cause to reduce $N(E_F)$ and (γ).

In addition, we have investigated the influence of pressure on the Fermi surface of CrF_3 therefore, to ascertain the effect of the pressure the Fermi surface of CrF_3 was calculated for the eight

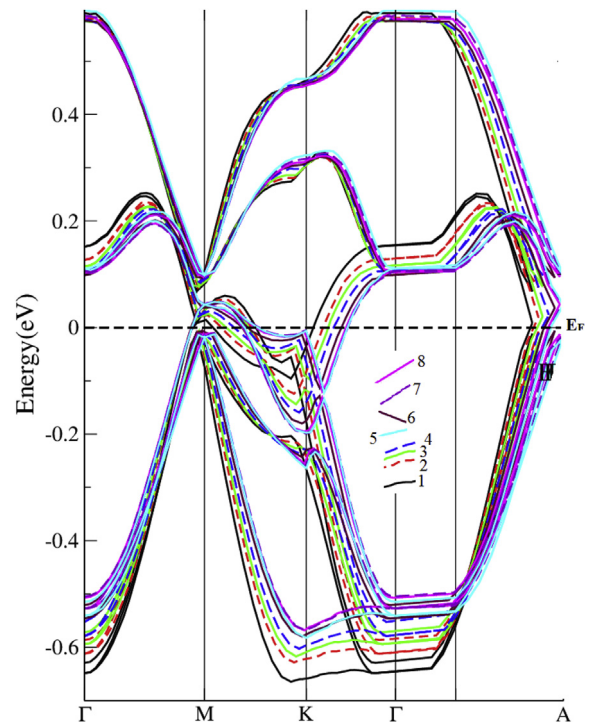


Fig. 3. Calculated electronic band structure for the pressure values 0.0001 GPa (case 1), 1.01 GPa (case 2), 1.84 GPa (case 3), 3.43 GPa (case 4), 5.43 GPa (case 5), 7.46 GPa (case 6), 8.56 GPa (case 7) and 9.12 GPa (case 8).

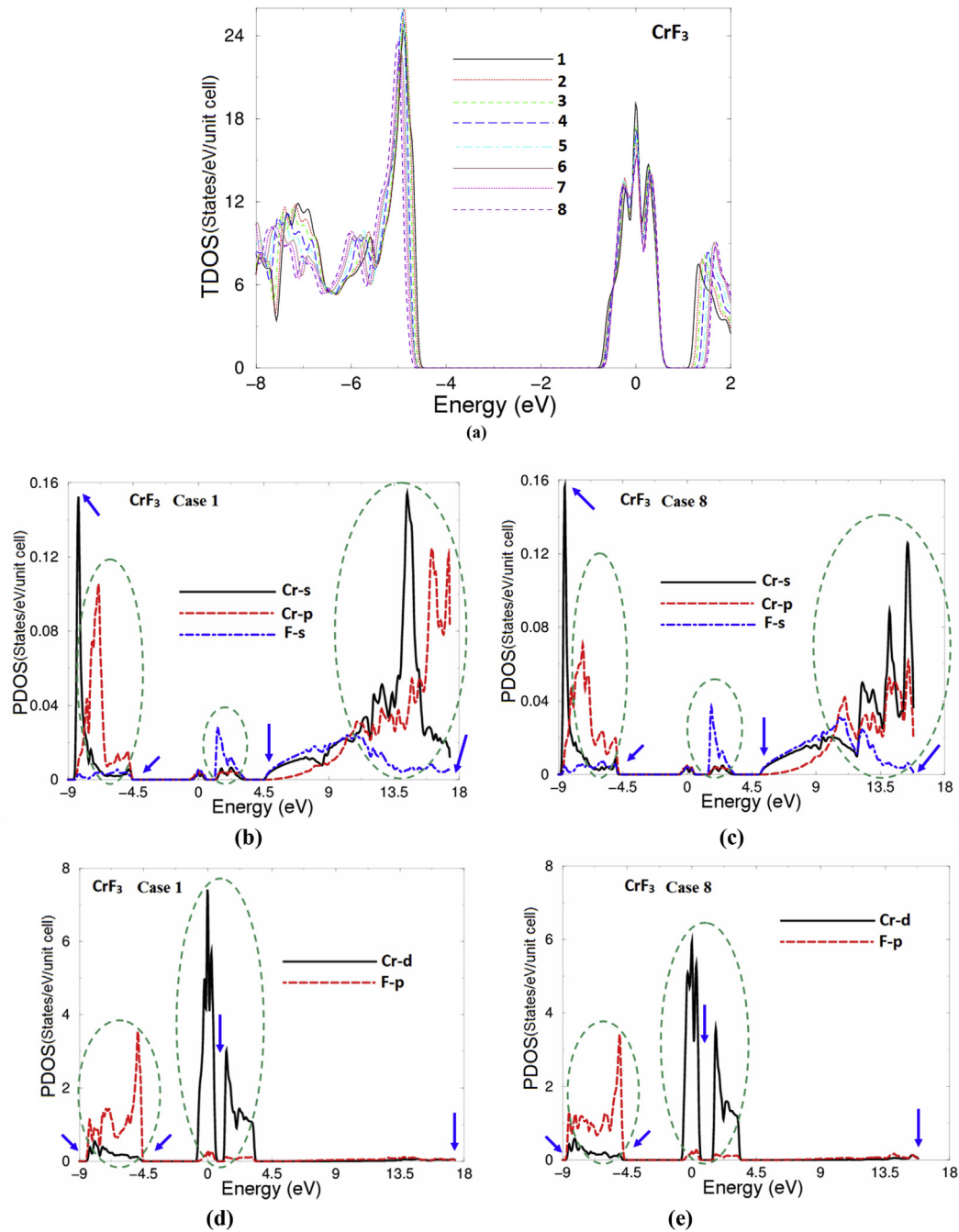


Fig. 4. (a) Calculated total density of states within the investigated pressure range. The calculated partial density of states of: (b) Cr-s/p and F-s at ambient pressure 0.0001 GPa; (c) Cr-s/p and F-s at high pressure 9.12 GPa; (d) Cr-d and F-p at ambient pressure 0.0001 GPa; (e) Cr-d and F-p at high pressure 9.12 GPa.

Table 1

The density of states at Fermi energy $N(E_F)$ states/Ry cell, the bare electronic specific heat coefficient γ (mJ/cell mole K^2) and γ (mJ/mole K^2).

P (GPa)	$N(E_F)$ states/Ry cell	γ (mJ/mole cell K^2)	γ mJ/mole K^2
0.0001	354.83	61.47	10.24
1.01	292.37	50.65	8.44
1.84	264.71	45.86	7.64
3.43	262.09	45.41	7.56
5.43	237.55	41.16	6.86
7.46	228.19	39.53	6.58
8.56	226.16	39.18	6.53
9.12	222.36	38.52	6.42

pressure values (eight cases) as shown in Fig. 5(a)–(h) and the Supplementary Materials Fig. S2(a) and (b). In all cases the Fermi surface is originated mainly from Cr-d states with small contribution of F-s/p and Cr-s/p states. From the calculated electronic band structure (Fig. 3) we can see that there are six bands crossing Fermi level to form the shape of Fermi surface. The Fermi surface of each band cuts E_F at ambient and high pressure are presented in the Supplementary Materials Fig. S2(a) and (b), it is clear that increasing the pressure cause significant influence on the shape of Fermi surface, that is attributed to the fact that shedding more pressure leads to change the locations of the bands at E_F , push the bands below and above E_F away from E_F below -4.0 eV and

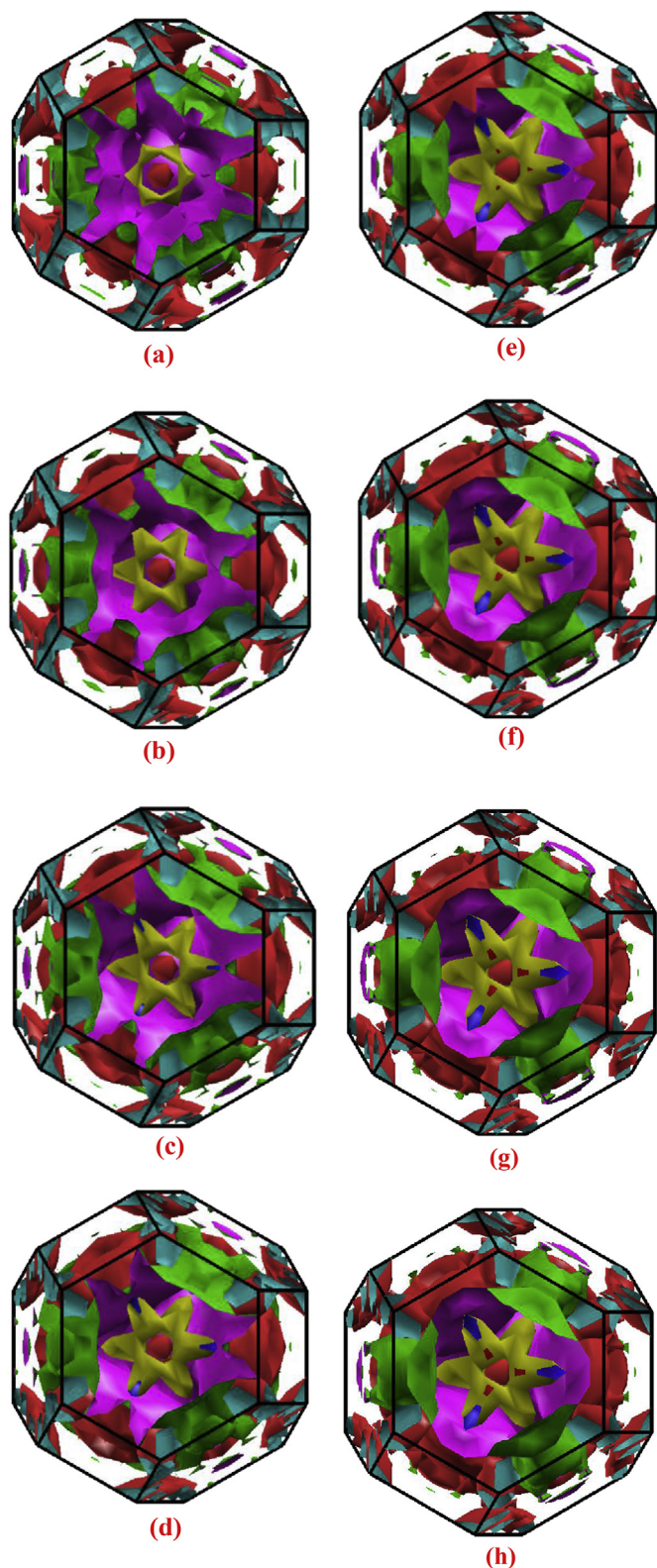


Fig. 5. Calculated Fermi surface for the pressure values; (a) 0.0001 GPa (case 1); (b) 1.01 GPa (case 2); (c) 1.84 GPa (case 3); (d) 3.43 GPa (case 4); (e) 5.43 GPa (case 5); (f) 7.46 GPa (case 6); (g) 8.56 GPa (case 7); (h) 9.12 GPa (case 8).

above -1.0 eV, resulting in change the shape of Fermi surface as shown in Fig. 5(a)–(h) and the Supplementary Materials Fig. S2(a) and (b). As we have mentioned before that the bonding states and anti-bonding states are closely related to the strength of the orbital

splitting. The external pressure leads to compress the chemical bonding and increase the orbital splitting. As consequence, the bonding states go deeper into the lower energy level and the energy level of the anti-bonding states enhanced resulting in some modification in the Fermi surface as shown in Fig. 5(a)–(h) and Fig. S2(a and b). Fermi surface consists of empty areas that represented the holes and shaded areas corresponding to the electrons.

In order to investigate the influence of increasing the pressure on the electronic charge distribution and the nature of the chemical bonding, we have calculated the total valence charge density distribution in (1 0 0) and (1 0 1) crystallographic planes at the investigated pressure values (eight cases), as prototype the case 1 and case 8 are shown in Fig. 6(a,b) and (c,d). The crystallographic plane (1 0 0) for case 1 and 8 show only Cr atoms which are surrounding by a uniform spherical charge confirming the ionic nature of Cr atoms. The distances between Cr–Cr in (1 0 0) plane is about 4.98 Å for case 1 and 4.62 Å for case 8, indicating that the pressure cause to compress the unit cell of CrF_3 by around 0.36 Å in the (1 0 0) direction. Following Fig. 6(c and d) it is clear that the (1 0 1) crystallographic plane exhibit all atoms. According to Pauling scale the electro-negativity of Cr and F is 1.66 and 3.98, therefore, due to the electro-negativity difference between Cr and F atoms one can see the charge transfer towards F atoms as indicated by the blue color around F atoms. The F atoms are surrounding by a uniform spherical charge indicating the ionic characters. The distance between Cr–Cr atoms in (1 0 1) plane is 3.62 Å for case 1 while it is 3.45 Å for case 8, thus the pressure cause to compress the unite cell of CrF_3 by around 0.17 Å in the (1 0 1) direction. The CrF_6 octahedron contains two F–F distances, these are denoted as d_1 and d_2 . The calculated d_1 and d_2 at ambient pressure are found to be $d_1 = 2.684$ Å and $d_2 = 2.693$ Å whereas at high pressure $d_1 = 2.640$ Å and $d_2 = 2.671$ Å in good agreement with the experimental data ($d_1 = 2.641$ (5) Å and $d_2 = 2.672$ (2) Å) [6]. The values of d_1 and d_2 for all eight cases (pressure values) are listed in Table 2 and illustrated in Fig. 7(a). It has been noticed that d_1 is reduced by 1.6% within the investigated pressure range and there is significant change in the slope of d_1 at 3.43 GPa, whereas d_2 is reduced by 0.80% and exhibit smooth decreasing during increasing the pressure, in good agreement with the experimental data [6]. From d_1 and d_2 one can obtain the values of the octahedral strain (ϵ) as shown in Table 2 and Fig. 7(b). It is clear that the values of ϵ increases linearly up to $\epsilon = 4.48 \times 10^{-3}$ at the pressure value 3.43 GPa which is in good agreement with the experimental value (4.5×10^{-3} @ 3.43 GaP) [6]. Then the ϵ tends to be constant above 3.43 GPa. That is attributed to the difference in the pressure dependence of d_1 and d_2 which lead to increasing the rhombohedral distortion of CrF_6 octahedra. It has been found that a small octahedral strain (ϵ) occurs when we move from 0.0001 GPa up to 9.12 GPa, the increasing of ϵ is in concordance with the pressure dependence of the c-lattice constant. The calculated ϵ show good agreement with the measured one [6] within the investigated pressure range. It is clear that Fig. 7(a) and (b) exhibit the structural changes of CrF_3 during compression, in good agreement with the experimental data [6].

The Cr–F bond lengths were calculated and compared to the experimental data [6], we found that the bond lengths of Cr–F are decreases by around 1.21% with increasing the pressure which agree well with the experimental data (1.2%) [6] (Table 2). The distances between Cr–Cr nearest neighbor were also calculated. It is clear that increasing the pressure cause to compress the Cr–Cr distance. In addition, the calculated bond angle Cr–F–Cr of CrF_6 octahedra decreases from 144.79° at ambient pressure to 133.88° at high pressure in good agreement with the experimental data [6] (Table 2).

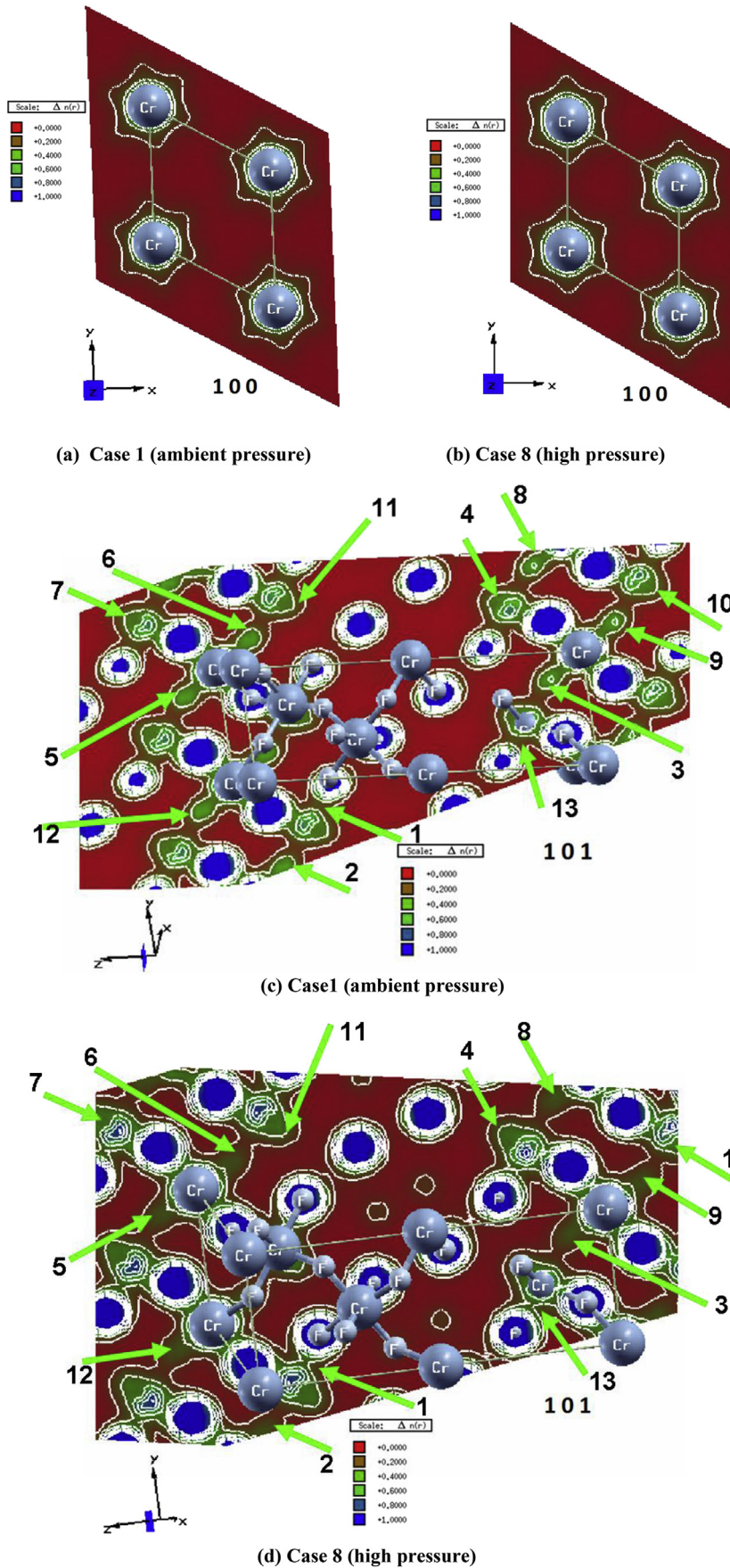


Fig. 6. Calculated electron charge density distribution were for; (a) (0 0 1) at ambient pressure 0.0001 GPa; (b) (0 0 1) at high pressure 9.12 GPa; (c) (1 0 1) at ambient pressure 0.0001 GPa; (d) (1 0 1) at high pressure 9.12 GPa. The influence of the pressure are marked by arrows and numbers, case 1 the ambient pressure case and case 8 is the high pressure case. For example one can see mark 1 and 13 which indicate that the high pressure force Cr atom to form partial covalent bond with F atom, in concordance with the our observation from the PDOS. According to the thermoscale the blue color exhibit the maximum charge accumulation. (For interpretation of the references to color in this figure legend, the reader is referred to the web version of this article.)

Table 2

The influence of compression on the strain $\varepsilon = (d_2 - d_1)/(d_2 + d_1)$, the Cr–Cr distances and the Cr–F, lengths of CrF₃ and Cr–F–Cr bond angles in comparison with the experimental data [6].

P (GPa)	d_1 (Å)	d_2 (Å)	ε	Cr–Cr (Å)	Cr–F (Å)	Cr–F–Cr ^o
0.0001	2.684	2.694	0.00185	4.986	1.901	144.78, 144.80(7)^a
1.01	2.682	2.693	0.00204	4.910	1.900	141.66
1.84	2.677	2.692	0.00279	4.859	1.899	139.95
3.43	2.666	2.690	0.00448	4.785	1.893	137.97
5.43	2.664	2.687	0.00429	4.718	1.891	135.62
7.46	2.658	2.681	0.00430	4.663	1.887	134.35
8.56	2.651	2.676	0.00469	4.638	1.883	134.05
9.12	2.640	2.671	0.00583	4.626	1.878	133.88, 133.9(4)^a
	2.641(5)^a	2.672(2)^a				

^a Ref. [6] (experimental value).

3.2. Linear optical properties

To further understand the influence of the pressure on the physical properties of CrF₃, the optical dielectric functions were calculated within the investigated pressure range. We should emphasize that the calculations of the optical dielectric functions involve the energy eigenvalues and electron wave functions which are natural outputs of band structure calculations. Hence, a clear picture can be gained from the optical transitions. It is clear from Fig. 8(a) and (b) at low energy (0.0–3.0 eV) increasing the pressure cause to shift the spectral features of $\varepsilon_2^{xx}(\omega)$ and $\varepsilon_2^{zz}(\omega)$ towards higher energies, whereas at the energy region (3.0–6.0 eV) the pressure leads to reduce the peak heights. It is interesting to see that at around 7.5 eV increasing the pressure cause to increase the peak heights of $\varepsilon_2^{xx}(\omega)$ and $\varepsilon_2^{zz}(\omega)$ components, while at high energies the pressure cause to reduce the peak heights and shift the spectral features towards higher energies. In general, the pressure causes significant influence on the spectral features of $\varepsilon_2^{xx}(\omega)$ and $\varepsilon_2^{zz}(\omega)$. Therefore, we selected to show the spectral features of $\varepsilon_2^{xx}(\omega)$ and $\varepsilon_2^{zz}(\omega)$ components for the ambient and high pressure as prototype. Fig. 8(c) and (d) illustrated the behaviors of $\varepsilon_2^{xx}(\omega)$ and $\varepsilon_2^{zz}(\omega)$ components at ambient pressure and 9.12 GPa. The spectral features at low energies (less than 1.0 eV) is due to the intra-band transitions. It has been found that the pressure cause to shift the spectral features of $\varepsilon_2^{xx}(\omega)$ and $\varepsilon_2^{zz}(\omega)$ which is located between 2.0 and 3.0 eV towards higher energies and splitting the peak of $\varepsilon_2^{zz}(\omega)$ into two small peaks. While it cause to reduce the peak heights at around 5.0 eV, increase the peak heights between 6.0 and 8.0 eV and reduce the peak heights of the spectral features around 9.0 eV. Also it has

been noticed that increasing the pressure leads to form a considerable anisotropy between $\varepsilon_2^{xx}(\omega)$ and $\varepsilon_2^{zz}(\omega)$ at low and high energies which makes CrF₃ a uniaxial crystal. In order to identify the spectral features of these optical components we need to look at the magnitude of the optical matrix elements. The observed structures of $\varepsilon_2^{xx}(\omega)$ and $\varepsilon_2^{zz}(\omega)$ would correspond to those transitions that have large optical matrix elements. Thus, these optical components completely define the linear optical properties. We have used the Kramers-Kronig transformation [24] to obtain the real parts of the optical dielectric functions.

Fig. 8(e) and (f) presented the real parts of the optical dielectric functions at ambient pressure and 9.12 GPa. It is clear that the pressure cause significant influence on the spectral features of $\varepsilon_1^{xx}(\omega)$ and $\varepsilon_1^{zz}(\omega)$ especially at low and high energy regions. Table 3 illustrated the influence of the compression on the calculated plasma frequency ω_p^{xx} and ω_p^{zz} which exhibit that the plasma frequencies are increases with increasing the pressure. Further deep insight into the electronic structure can be obtained by calculating the loss function $L(\omega)$, absorption coefficients $I(\omega)$ and the reflectivity spectra $R(\omega)$. These can be obtained from the imaginary and real parts of the optical dielectric functions. Fig. 8(g) and (h) present the loss function at ambient and high pressure. The observed pronounced peaks represent the plasma frequencies (ω_p^{xx} and ω_p^{zz}) which confirm the existence of the lossless regions at low and high energies as it has been shown in Fig. 8(a) and (b). The calculated absorption coefficients as shown in Fig. 8(i) and (j) exhibit that there exists low absorption regions which is located between 0.0 and 3.0 eV and high absorption region (8.0–13.5 eV). In these two regions the material exhibits high transparency. Fig. 8(k) and (l) present the reflectivity spectra, it illustrate that CrF₃ show high

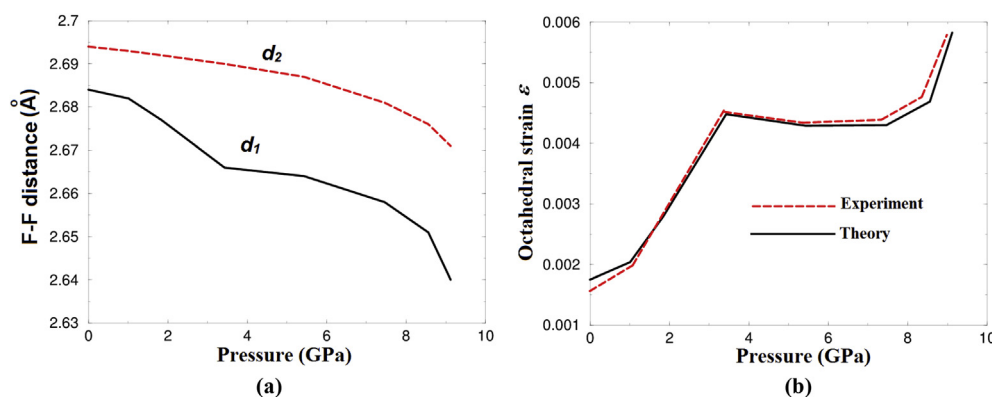


Fig. 7. (a) The calculated F–F distance (d_1 and d_2) as function of pressure; (b) Calculated octahedral strain as function of pressure in comparison with the measured one [6].

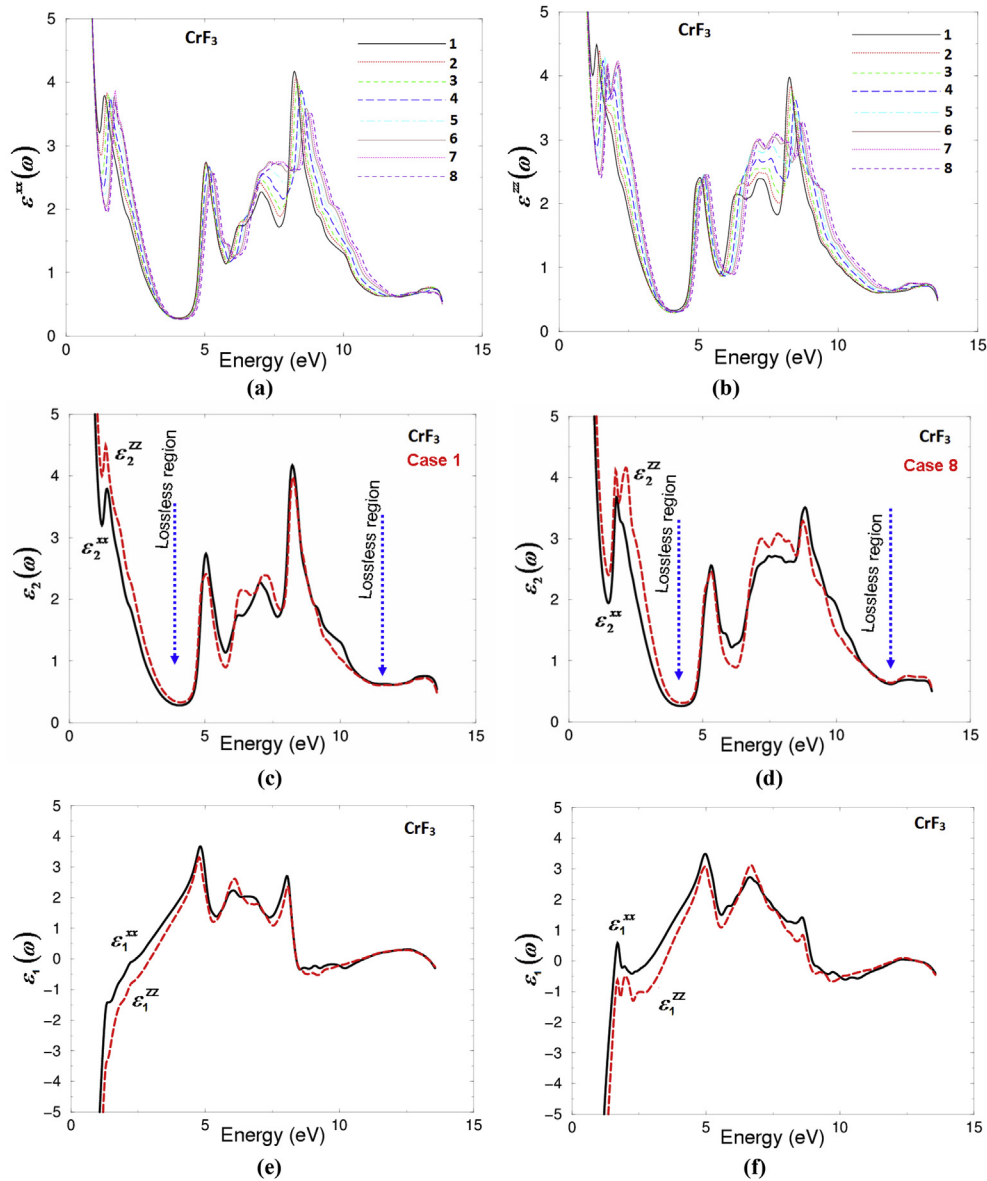


Fig. 8. (a) Calculated $\varepsilon_2^{xx}(\omega)$ for eight pressure values; (b) Calculated $\varepsilon_2^{zz}(\omega)$ for eight pressure values; (c) Calculated $\varepsilon_2^{xx}(\omega)$ and $\varepsilon_2^{zz}(\omega)$ at ambient pressure; (d) Calculated $\varepsilon_2^{xx}(\omega)$ and $\varepsilon_2^{zz}(\omega)$ at high pressure; (e) Calculated $\varepsilon_1^{xx}(\omega)$ and $\varepsilon_1^{zz}(\omega)$ at ambient pressure; (f) Calculated $\varepsilon_1^{xx}(\omega)$ and $\varepsilon_1^{zz}(\omega)$ at high pressure; (g) Calculated $L^{xx}(\omega)$ and $L^{zz}(\omega)$ at ambient pressure; (h) Calculated $L^{xx}(\omega)$ and $L^{zz}(\omega)$ at high pressure; (i) Calculated $R^{xx}(\omega)$ and $R^{zz}(\omega)$ at ambient pressure; (j) Calculated $R^{xx}(\omega)$ and $R^{zz}(\omega)$ at high pressure; (k) Calculated $R^{xx}(\omega)$ and $R^{zz}(\omega)$ at ambient pressure; (l) Calculated $R^{xx}(\omega)$ and $R^{zz}(\omega)$ at high pressure.

reflectivity below 1.0 eV, then drop to form the first reflectivity minima confirming the occurrence of collective plasmon resonance. It is clear that the pressure cause significant influence on the whole structure of the reflectivity spectra.

4. Conclusions

The calculated electronic band structure, density of states, electronic charge density, Fermi surface and the optical properties exhibit that the pressure have significant influence on the structural parameters and hence on the resulting properties. The calculated electronic band structure and Fermi surface show that there are six bands cross Fermi level, the pressure cause significant influence on the locations of these six bands. The CrF_6 octahedron contains two F–F distances (d_1 and d_2). The calculated d_1 and d_2 at ambient pressure are found to be $d_1 = 2.684 \text{ \AA}$ and $d_2 = 2.693 \text{ \AA}$

whereas at high pressure $d_1 = 2.640 \text{ \AA}$ and $d_2 = 2.671 \text{ \AA}$ in good agreement with the experimental data ($d_1 = 2.641 (5) \text{ \AA}$ and $d_2 = 2.672 (2) \text{ \AA}$). From d_1 and d_2 we have obtained the values of the octahedral strain ε which increases linearly up to $\varepsilon = 4.48 \times 10^{-3}$ at the pressure value 3.43 GPa in good agreement with the experimental value (4.5×10^{-3} @ 3.43 GPa) and small ε occurs with increasing the pressure. It has been found that increasing the pressure cause to reduce the bond lengths of Cr–F by around 1.21% which agree well with the experimental data (1.2%). The calculated bond angle Cr–F–Cr of CrF_6 octahedra decreases from 144.79° at ambient pressure to be 133.88° at high pressure in good agreement with the experimental data. The calculated imaginary part of the optical dielectric functions, loss functions and the reflectivity spectra exhibit that there exists two lossless regions, while the absorption coefficient show two absorption regions within the investigated pressure range.

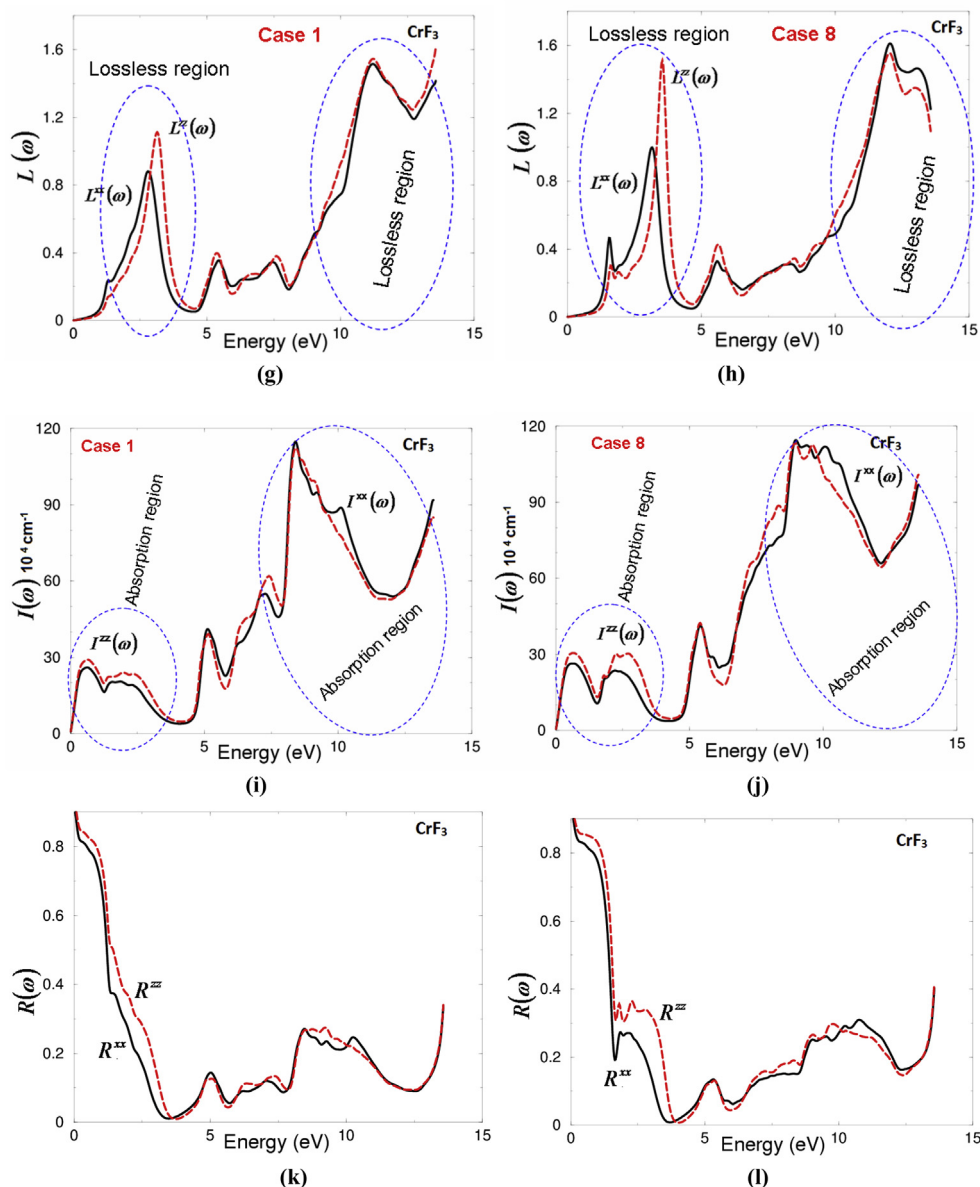


Fig. 8. (continued).

Table 3

The influence of compression on the plasma frequency.

P (GPa)	ω_p^{xx}	ω_p^{zz}
0.0001	1.7343	2.2311
1.01	1.8286	2.4154
1.84	1.9017	2.5302
3.43	2.0211	2.6719
5.43	2.0986	2.7310
7.46	2.1963	2.7376
8.56	2.2314	2.7557
9.12	2.2353	2.7891

Acknowledgments

The result was developed within the CENTEM project, reg. no. CZ.1.05/2.1.00/03.0088, cofunded by the ERDF as part of the Ministry of Education, Youth and Sports OP RDI programme and, in the follow-up sustainability stage, supported through CENTEM PLUS

(LO1402) by financial means from the Ministry of Education, Youth and Sports under the "National Sustainability Programme I. Computational resources were provided by MetaCentrum (LM2010005) and CERIT-SC (CZ.1.05/3.2.00/08.0144) infrastructures.

Appendix A. Supplementary data

Supplementary data related to this article can be found at <http://dx.doi.org/10.1016/j.jallcom.2015.11.035>.

References

- [1] F.H. Herbstein, M. Kapon, G.M. Reisner, Z. Kristallogr. 171 (1985) 209.
- [2] Gerd Anger, Jost Halstenberg, Klaus Hochgeschwender, Christoph Scherhag, Ulrich Korallus, Herbert Knopf, Peter Schmidt, Manfred Ohlinger, Chromium Compounds, in: Ullmann's encyclopedia of industrial chemistry, Wiley-VCH, Weinheim, 2005, http://dx.doi.org/10.1002/14356007.a07_067.
- [3] N.N. Greenwood, A. Earnshaw, Chemistry of the Elements, second ed., Butterworth-Heinemann, Oxford, 1997. ISBN:0-7506-3365-4.

- [4] K.H. Jack, R. Maitland, Proc. Chem. Soc. Lond. (1957), 232–232.
- [5] K. Knox, Acta Cryst. 13 (1960) 507–508.
- [6] J.-E. Jorgensen, W.G. Marshall, R.I. Smith, Acta Cryst. B 60 (2004) 669–673.
- [7] W. Fischer, Z. Krist. 138 (1973) 129–146.
- [8] K. Meisel, Z. Anorg. Allg. Chem. 207 (1932) 121–128.
- [9] P. Herzig, J. Zemann, Z. Krist. 205 (1993) 85–97.
- [10] R. von Losch, ch Hebecher, Z. Ranft, Z. Anorg. Allg. Chem. 491 (1982) 199–202.
- [11] M.A. Hepworth, K.H. Jack, R.D. Peacock, G.J. Westland, Acta Cryst. 10 (1957) 63–69.
- [12] L. Grosse, R. Hoppe, Z. Anorg. Allg. Chem. 552 (1987) 123–131.
- [13] H. Sowa, H. Ahsbahs, Acta Cryst. B 54 (1998) 578–584.
- [14] J.-E. Jorgensen, J.S. Olsen, L. Gerward, J. Appl. Cryst. 33 (2000) 279–284.
- [15] G. Lakshminarayana, Rong Yang, Mengfei Mao, Jianrong Qiu, I.V. Kityk, J. Non-Crystall. Solids 355 (2009) 2668–2673.
- [16] A.H. Reshak, RSC Adv. 5 (2015) 47569.
- [17] K.J. Plucinski, I.V. Kityk, J. Kasperczyk, B. Sahraoui, Semicond. Sci. Technol. 16 (2001) 467–470.
- [18] M. Malachowski, I.R. Kityk, B. Sahraoui, Phys. Lett. A 242 (1998) 337–342.
- [19] A.H. Reshak, A. Majchrowski, M. Swirkowicz, A. Kłos, T. Łukasiewicz, I.V. Kityk, K. Iliopoulos, S. Couris, M.G. Brik, J. Alloys Compd. 481 (2009) 14–16.
- [20] A.H. Reshak, S. Auluck, I.V. Kityk, J. Alloys Compd. 473 (2009) 20–24.
- [21] J.P. Perdew, S. Burke, M. Ernzerhof, Phys. Rev. Lett. 77 (1977) 3865.
- [22] P. Blaha, K. Schwarz, G.K.H. Madsen, D. Kvasnicka, J. Luitz, WIEN2k, an Augmented Plane Wave Plus Local Orbitals Program for Calculating Crystal Properties, Vienna University of Technology, Austria, 2001.
- [23] A.H. Reshak, Z. Charifi, H. Baaziz, J. Solid State Chem. 183 (2010) 1290–1296.
- [24] F. Wooten, Optical Properties of Solids, Academic Press, New York and London, 1972.